NANO LETTERS

LETTER

pubs.acs.org/NanoLett

Nanofabrication of Heteromolecular Organic Nanostructures on Epitaxial Graphene via Room Temperature Feedback-Controlled Lithography

Qing Hua Wang[†] and Mark C. Hersam*[,†,‡]

[†]Department of Materials Science and Engineering, Northwestern University, Evanston, Illinois 60208, United States

[‡]Department of Chemistry, Northwestern University, Evanston, Illinois 60208, United States

Supporting Information

ABSTRACT: Nanoscale control of surface chemistry holds promise for tailoring the electronic, optical, and chemical properties of graphene. Toward this end, the nanofabrication of sub-5-nm heteromolecular organic nanostructures is demonstrated on epitaxial graphene using room temperature ultrahigh vacuum scanning tunneling microscopy. In particular, monolayers of the organic semiconductor 3,4,9,10-perylene-tetracarboxylic dianhydride (PTCDA) are nanopatterned on epitaxial graphene using feedback-controlled lithography (FCL) and then used as chemical resists to template the deposition of *N*,*N*′-dioctyl-3,4,9,10-perylene-tetracarboxylic diimide (PTCDI-C8). The generality of this FCL-based nanofabrication procedure suggests its applicability to a wide range of fundamental studies and prototype device fabrication on chemically functionalized graphene.

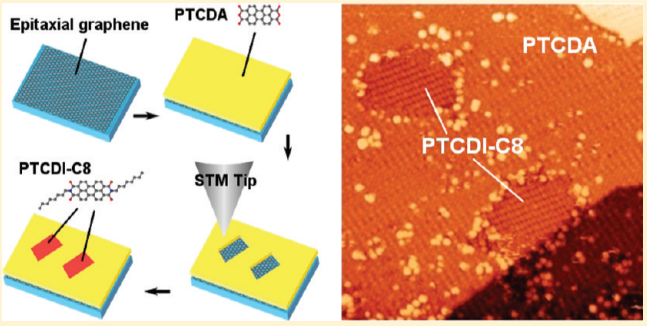

KEYWORDS: Graphene, scanning tunneling microscopy, nanolithography, self-assembled monolayer, organic functionalization

The extraordinary electronic properties of graphene[1,2] make it an attractive material for next generation electronics.[3] While many promising electronic[4] and sensing devices[5,6] have been demonstrated, important challenges remain including interfacing graphene with dielectrics and organics, controlling the band gap and doping of graphene, and high-resolution lithography.[7] Chemical functionalization of graphene has been pursued via a variety of covalent and noncovalent schemes. Covalent attachment of species such as oxygen,[8] hydrogen,[9−11] and aryl groups[12] generally disrupts the electronic properties of graphene. On the other hand, noncovalent chemistries allow for less perturbative tuning of the doping and surface reactivity of graphene. For example, noncovalently interacting species have been demonstrated to act as dopants,[13,14] solubilizing agents,[15,16] and nucleation layers for the deposition of dielectric films.[17]

Lithographic patterning of graphene is actively being explored for the nanofabrication of graphene nanoribbons and for the local modification of graphene surface chemistry. Several groups have nanopatterned graphene using scanning probe microscopy techniques.[9,18−21] These early results have focused on covalent modification of graphene with an eye toward fabricating graphene nanoribbons.[19,21] While evidence of quantum confinements effects has been reported in these SPM-patterned nanoribbon structures, line width control has been limited by patterning resolution and/or the lack of uniform covalent modification. Furthermore, nanoscale templating of subsequent chemistry has not yet been demonstrated.

Here, we demonstrate the nanofabrication of sub-5-nm heteromolecular organic nanostructures on epitaxial graphene grown on SiC(0001) using room temperature ultrahigh vacuum (UHV) scanning tunneling microscopy (STM). In particular, the organic semiconductor 3,4,9,10-perylene-tetracarboxylic dianhydride (PTCDA), which forms well-ordered monolayers on graphene,[22−24] is nanopatterned by feedback-controlled lithography (FCL) and then used as a chemical resist to template the deposition of *N*,*N*′-dioctyl-3,4,9,10-perylene-tetracarboxylic diimide (PTCDI-C8). Using molecular-resolution UHV STM, the role of intermolecular interactions in the geometry, growth mode, and stability of the PTCDA/PTCDI-C8 heteromolecular nanostructures is delineated. Nanopatterned organically functionalized graphene enables fundamental studies and prototype device fabrication, thus facilitating ongoing efforts to realize graphene-based technology.

Epitaxial graphene was prepared on 6H-SiC(0001) substrates (Cree, Inc.) by heating the samples above 1300 °C for several cycles of 60 s in UHV. Subsequent room temperature STM characterization of the samples was accomplished in the same home-built UHV system[25] and employed electrochemically etched W tips. STM imaging at many locations across the sample

Received: October 12, 2010
Revised: November 29, 2010
Published: December 17, 2010

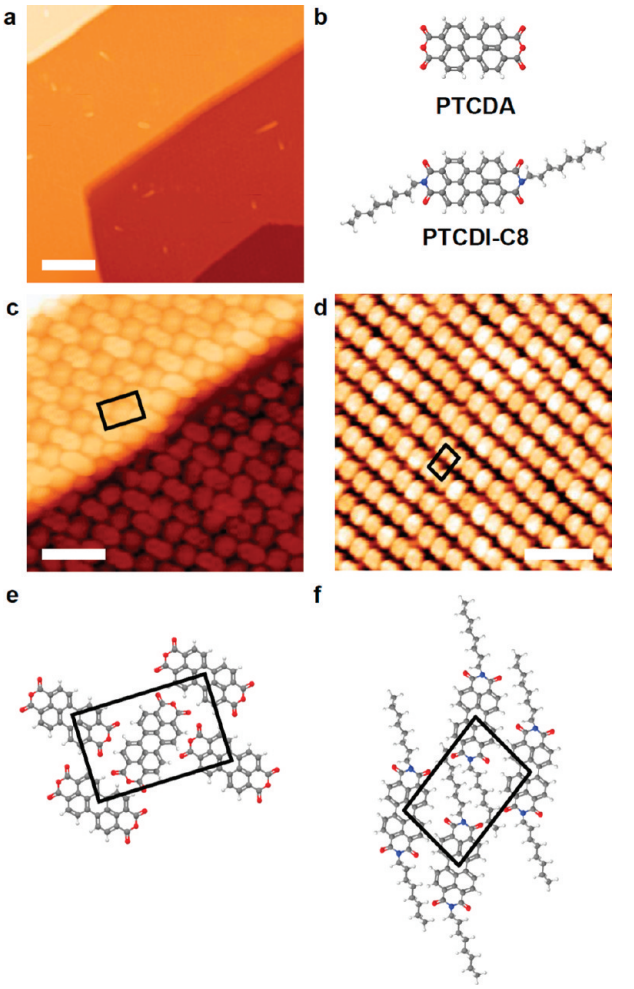

Figure 1. Organic monolayers on epitaxial graphene. (a) Room temperature STM image of the initial pristine epitaxial graphene surface (Imaging conditions: sample bias $V_s = -2.0$ V, tunneling current $I_t = 0.05$ nA, scale bar 15 nm). (b) Molecular structures of 3,4,9,10-perylene-tetracarboxylic dianhydride (PTCDA) and *N*,*N*′-dioctyl-3,4,9,10-perylene-tetracarboxylic diimide (PTCDI-C8). Gray, red, and blue spheres are C, O, and N respectively. (c) PTCDA monolayer assembled on epitaxial graphene ($V_s = -2.0$ V, $I_t = 0.07$ nA, scale bar 3 nm). (d) PTCDI-C8 monolayer assembled on epitaxial graphene ($V_s = -1.0$ V, $I_t = 0.05$ nA, scale bar 5 nm). (e) Schematic model of the PTCDA monolayer unit cell. (f) Schematic model of the PTCDI-C8 monolayer unit cell.

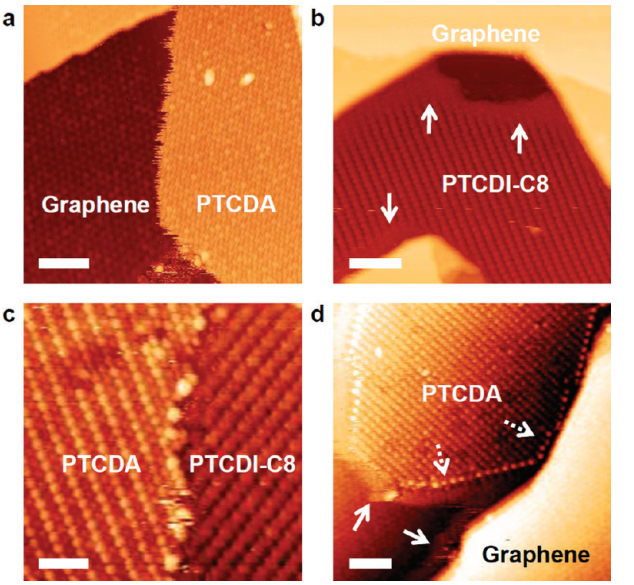

Figure 2. Interaction of PTCDA and PTCDI-C8 monolayers. (a) Room temperature STM image of a submonolayer island of PTCDA, showing a disordered domain boundary on graphene ($V_s = -2.0$ V, $I_t = 0.05$ nA, scale bar 10 nm). (b) A submonolayer PTCDI-C8 island shows boundaries that appear to fade into the graphene background, as indicated with arrows ($V_s = -2.0$ V, $I_t = 0.05$ nA, scale bar 10 nm). (c) Clearly defined boundary between a PTCDA domain and a PTCDI-C8 domain ($V_s = -2.0$ V, $I_t = 0.05$ nA, scale bar 5 nm). (d) During the initial stages of deposition onto a submonolayer PTCDA sample, PTCDI-C8 preferentially accumulates at the edges of existing features such as PTCDA islands and graphene step edges, as indicated with solid arrows. The edges of the PTCDA island are decorated with PTCDI-C8 molecules, which appear as brighter spots that stabilize the PTCDA boundary, as indicated with dashed arrows ($V_s = -1.5$ V, $I_t = 0.04$ nA, scale bar 10 nm).

showed a mixture of single layer and bilayer graphene domains, which can be visually distinguished by their differing roughness and apparent topographic contrast.[22] A typical clean epitaxial graphene surface is shown in the room temperature UHV STM image of Figure 1a.

Self-assembled monolayers of PTCDA (97% purity, Sigma-Aldrich) and PTCDI-C8 (98% purity, Sigma-Aldrich) were formed on graphene by thermal evaporation in UHV from alumina-coated W boats (Midwest Tungsten Service). The molecules, whose structures are shown in Figure 1b, both form well-ordered monolayers on graphene. For PTCDA, herringbone ordering is observed (Figure 1c,e) due to hydrogen bonding between adjacent molecules,[22] while the aromatic backbone is noncovalently bound to the graphene sheet via $\pi-\pi^*$ interactions. The PTCDA monolayer interacts weakly with the epitaxial graphene and, unlike its behavior on highly ordered pyrolytic graphite (HOPG), is insensitive to surface defects and step edges.[22,24] Consequently, PTCDA forms highly ordered and uniform monolayers on epitaxial graphene that are the ideal starting point for a molecular resist. For PTCDI-C8 (Figure 1d), the alkyl chains weaken the intermolecular interactions, leading to rectangular symmetry in the self-assembled monolayer. This symmetry is consistent with a previous study of PTCDI-alkyl derivatives,[26] suggesting that the aromatic backbone lies flat on the graphene surface while the alkyl chains protrude above the plane of the backbone (Figure 1f).

At submonolayer coverage, PTCDA and PTCDI-C8 form molecular islands that have different edge behavior. The PTCDA island edge (Figure 2a) is sharp and distinct from the graphene background, although there is some instability during STM imaging since the outer molecules have fewer nearest neighbors to stabilize them. In contrast, as indicated by the arrows in Figure 2b, the PTCDI-C8 island edge is ill-defined and indistinct, with the molecules appearing to fade into the graphene background. This difference can likely be attributed to the weaker intermolecular interactions in the PTCDI-C8 monolayer, which implies greater molecular diffusion at the PTCDI-C8 island edge.

The interaction between PTCDA and PTCDI-C8 domains is shown in Figure 2c,d. After ~0.5 monolayers (ML) of PTCDA and ~0.5 ML of PTCDI-C8 are sequentially deposited, separate domains of each molecule are observed (Figure 2c). The PTCDI-C8 fills in the remaining graphene areas that are not

dx.doi.org/10.1021/nl103590j |*Nano Lett.* 2011, 11, 589–593

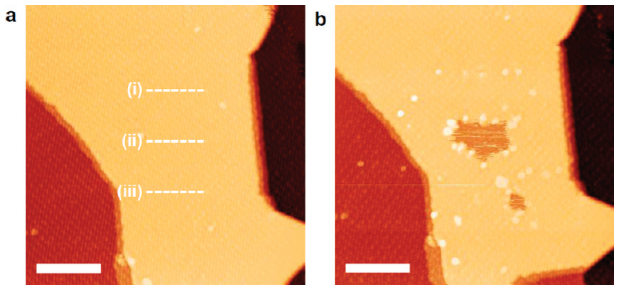

Figure 3. Nanopatterning PTCDA without FCL. (a, b) STM images of a PTCDA monolayer on epitaxial graphene (a) before and (b) after nanopatterning lines without a secondary feedback loop. In (a), the dotted lines indicate the paths taken by the tip during nanopatterning (−3.6 V, 0.5 nA, tip speed 23 nm/s). The resulting patterns in (b) are inconsistent: the top pattern shows no desorption, the middle pattern is 10−15 nm wide, and the bottom pattern is a sub-5-nm dot. For both images, V_s = −2.0 V, I_t = 0.04 nA, and scale bars are 20 nm.

covered by PTCDA rather than depositing on top of the PTCDA layer, which is consistent with the known growth mode of PTCDA on graphene, where a full monolayer is formed before the growth of a second molecular layer.[24] In Figure 2d, the early stage of PTCDI-C8 growth on a ∼0.5 ML PTCDA graphene surface is imaged, showing the nucleation of PTCDI-C8 at the edges of PTCDA islands and graphene/SiC steps. The growing PTCDI-C8 film appears as a bright, ill-defined band (solid arrows) except at the boundary of the PTCDA island, where the PTCDI-C8 molecules interact strongly enough with the PTCDA molecules to stabilize the interface and produce a distinct line of bright features (dashed arrows). The previously unstabilized PTCDA edge molecules are now stabilized interior molecules, while the edge is now comprised of unstabilized PTCDI-C8 molecules. Furthermore, the presence of PTCDI-C8 has caused the interface between PTCDA and PTCDI-C8 to adopt a lower energy configuration and rearrange the interface into straight lines.

The ability of PTCDA to adopt distinct boundaries indicated its suitability for supporting nanoscale features. Initially, we attempted to nanopattern the PTCDA monolayer by scanning the STM tip across the PTCDA monolayer along the three dotted lines in Figure 3a while applying an elevated bias and current (−3.6 V sample bias, 0.5 nA tunneling current, 23 nm/s tip speed). We then reimaged the same area at nonperturbative conditions (−2.0 V, 0.04 nA) as shown in Figure 3b. While selective desorption of small regions of the PTCDA monolayer is observed, the results are inconsistent. At position (i) no PTCDA desorption was achieved, while at position (ii) a relatively large patch of PTCDA was removed, leaving a pattern with width of 10−15 nm, and at position (iii) a small dot less than 5 nm was formed.

To improve the reliability, reproducibility, and resolution of the PTCDA nanopatterning, we employed feedback-controlled lithography (FCL).[27−30] FCL employs a secondary feedback loop to detect changes in the tunneling current indicative of molecular desorption during nanopatterning. In this manner, nanopatterning is terminated immediately following the desorption event, preventing additional desorption and thus minimizing the nanopattern size. Furthermore, since nanopatterning continues until desorption occurs, FCL is relatively insensitive to changes in the tip−sample junction that likely explain the inconsistent results observed in Figure 3. In Figure 4, FCL was

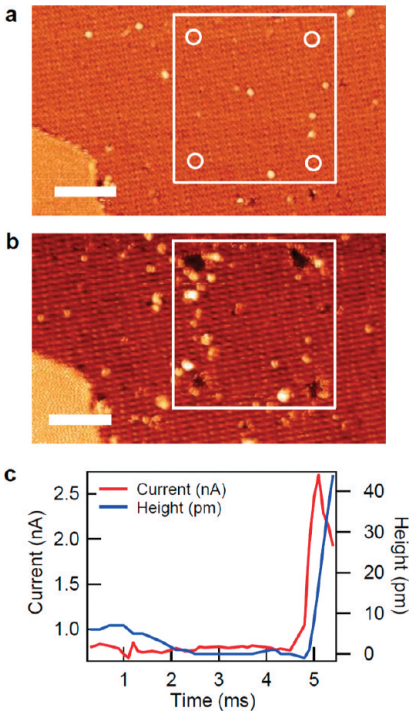

Figure 4. Nanopatterning PTCDA by FCL. (a, b) STM images of a PTCDA monolayer (a) before and (b) after nanopatterning by FCL. The FCL nanopatterning locations are indicated by circles in (a). The patterning conditions were −4.0 V, 0.3 nA (both images: V_s = −1.85 V, I_t = 0.04 nA, scale bars 15 nm). (c) Plots of tunneling current (red line) and change in tip height (blue line) vs time during FCL. Upon application of the FCL patterning conditions, a secondary feedback loop detects a sharp spike in the tunneling current followed by an increase in the tip height and subsequently terminates the patterning conditions.

used to pattern four dots at −4.0 V applied bias, 0.3 nA tunneling current, and a threshold condition of 13% change in current. The resulting patterns in Figure 4b are each about 4−5 nm in diameter and are consistent in shape and positioning. During FCL, the tunneling current and tip height are recorded as a function of time as shown in Figure 4c. A sharp increase in the current is detected indicating a successful desorption event, followed by a similar increase in the tip height as the primary feedback loop reestablishes the nanopatterning set point condition. An increase in current is observed for PTCDA desorption, rather than a decrease as might be expected for the formation of a topographic depression. We believe this effect can be attributed to the increased density of states of pristine graphene compared to PTCDA at the nanopatterning conditions (−4.6 V, 0.5 nA) or to desorbed PTCDA molecules that are briefly trapped in the tip−sample junction. Following extensive exploration of the nanopatterning phase space, the most critical parameter is the sample bias; namely, desorption readily occurs for sample biases exceeding −4.0 ± 0.5 V. The FCL nanopatterning current and secondary feedback loop cutoff conditions also provide control over the nanopattern size. In particular, FCL near the nanopatterning threshold shows sub-2-nm nanopatterning resolution (see Figure S1 of the Supporting Information).

Using the chemical insight gained from Figure 2, the nanopatterned PTCDA monolayer was used as a chemical template following the procedure schematically illustrated in Figure 5a. The implementation of this schematic is shown in the STM

dx.doi.org/10.1021/nl103590j |*Nano Lett.* 2011, 11, 589–593

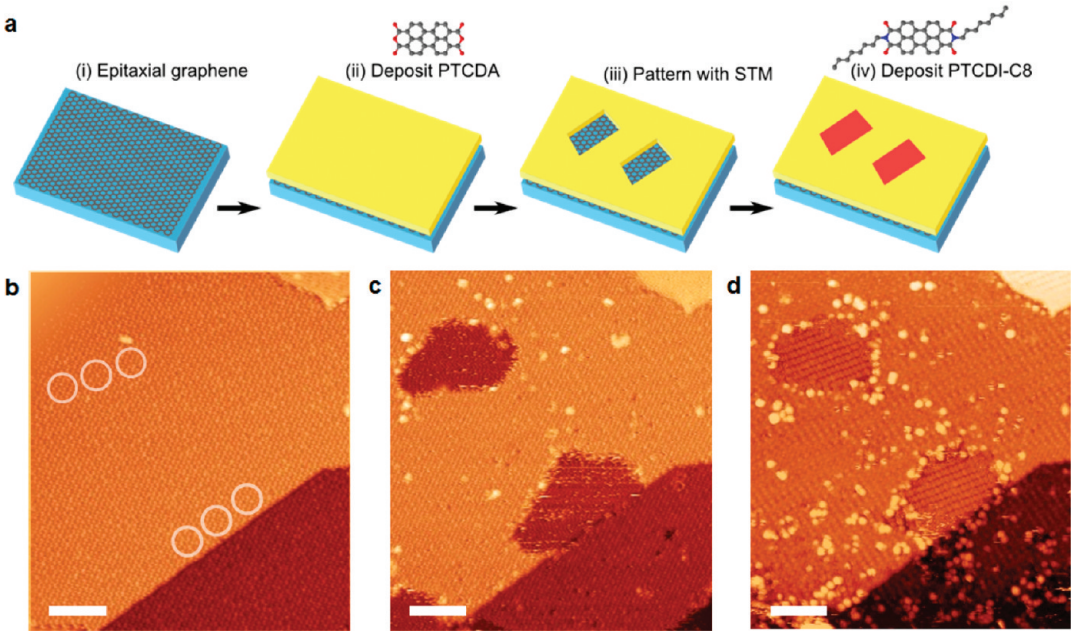

Figure 5. Heteromolecular nanopatterns. (a) Schematic illustration of the formation of heteromolecular nanopatterns. Step (i), clean epitaxial graphene on SiC(0001). Step (ii), deposition of PTCDA to form a monolayer. Step (iii), patterning of the PTCDA monolayer using FCL to expose clean graphene. Step (iv), deposition of PTCDI-C8 onto the exposed graphene regions with the PTCDA layer acting as a chemical resist. (b, c, and d) STM images showing implementation of the patterning and deposition, corresponding to steps (ii), (iii), and (iv), respectively. Patterning conditions to create the features in (c) were −4.6 V, 0.5 nA, with the locations of the FCL dots indicated as circles in (b). For all STM images, $V_s = -1.8$ V, $I_t = 0.02$ nA, and scale bars are 10 nm.

images of Figure 5b−d. A clean PTCDA monolayer (Figure 5b) was patterned by a series of closely spaced FCL dots to form two larger regions of exposed graphene (Figure 5c). PTCDI-C8 was then thermally evaporated in situ to fill in the patterns (Figure 5d). Deposition of PTCDI-C8 was accomplished by firmly packing the PTCDI-C8 powder into a 0.02 in. diameter alumina tube (Omega Engineering, Inc.), which was then wrapped with a 0.25 mm diameter Ta wire for resistive heating in situ. The PTCDI-C8 completely fills the two nanopatterns, forming a well-ordered nanoscale domain within the PTCDA monolayer. The emergence of molecular ordering within a patterned region with increasing PTCDI-C8 dose is shown in Figure S2 of the Supporting Information.

As the sample progresses from the initial PTCDA monolayer to the final heteromolecular nanopattern, the number of point defects is observed to increase. In particular, immediately after nanopatterning, additional bright features are seen outside of the nanopatterns (Figure 5c) that are attributed to PTCDA molecules that have readsorbed to the surface following FCL-driven desorption. Additional dark point defects are also observed and appear to be single missing PTCDA molecules that emerge as the monolayer is disrupted during nanopatterning. Following PTCDI-C8 deposition, additional bright features outside of the nanopatterns in Figure 5d are presumably PTCDI-C8 molecules that have adsorbed at the defects already present in Figure 5c. The shape of the nanopatterns also undergoes changes from Figure 5c to 5d. Both nanopatterns are elongated and anisotropic immediately after nanolithography (Figure 5c) but become more rounded and isotropic after PTCDI-C8 deposition (Figure 5d). However, the surface area of the patterns is not significantly changed (i.e., the upper pattern maintains the same area and the lower pattern is only about 10% smaller). The change in shape without significant changes in area can be attributed to (1) rearrangement of PTCDA/PTCDI-C8 boundaries to the low-energy configurations that were noted in Figure 2d and (2) radiative sample heating during PTCDI-C8 deposition that drives molecular diffusion. The net effect is a relatively symmetric nanoscale heteromolecular nanostructure with well-defined edges, which is desirable for envisioned graphene-based quantum devices where edge effects play a significant role.[31]

In conclusion, we have studied self-assembled monolayers of PTCDA and PTCDI-C8 on epitaxial graphene using room temperature UHV STM. The intermolecular forces in these noncovalent monolayers play a central role in the geometry and stability of heteromolecular domain boundaries. Informed by this molecular-level characterization, room temperature FCL is employed to desorb PTCDA from graphene at the sub-5-nm length scale. The resulting nanopatterns are subsequently used to template PTCDI-C8, thus demonstrating the utility of PTCDA as a chemical resist. The high resolution nanoscale patterning of the PTCDA chemical resist can likely be used as a template for further chemical functionalization, including covalent or etching chemistries that could provide a means for nanopatterning the graphene substrate itself. Ultimately, the ability to fabricate well-defined heteromolecular nanopatterns creates opportunities for future studies of graphene physics, chemistry, functionalization, and applications.

■ ASSOCIATED CONTENT

Supporting Information. Detailed experimental methods and materials, STM data showing voltage and current dependence of FCL patterning, and STM images showing the emergence of ordering in heteromolecular patterns. This material is available free of charge via the Internet at http://pubs.acs.org.

dx.doi.org/10.1021/nl103590j |*Nano Lett.* 2011, 11, 589–593

AUTHOR INFORMATION

Corresponding Author

*Address: Northwestern University, Department of Materials Science and Engineering, 2220 Campus Drive, Evanston, IL, 60208. Tel: (847) 491-2696. FAX: (847) 491-7820. E-mail: m-hersam@northwestern.edu.

ACKNOWLEDGMENT

This work was supported by the National Science Foundation (Award Numbers EEC-0647560 and DMR-0520513), the Office of Naval Research (Award Number N00014-09-1-0180), and the Department of Energy (Award Number DE-SC0001785). The authors thank M.A. Walsh for helpful discussions, A.A. Green for assistance with image analysis, and J.W. Lyding for use of his STM control software.

REFERENCES

(1) Bolotin, K. I.; Sikes, K. J.; Jiang, Z.; Klima, M.; Fudenberg, G.; Hone, J.; Kim, P.; Stormer, H. L. *Solid State Commun.* **2008,** *146,* 351.

(2) Du, X.; Skachko, I.; Barker, A.; Andrei, E. Y. *Nat. Nanotechnol.* **2008,** *3,* 491.

(3) Geim, A. K. *Science* **2009,** *324,* 1530.

(4) Lin, Y. M.; Dimitrakopoulos, C.; Jenkins, K. A.; Farmer, D. B.; Chiu, H. Y.; Grill, A.; Avouris, P. *Science* **2010,** *327,* 662.

(5) Cohen-Karni, T.; Qing, Q.; Li, Q.; Fang, Y.; Lieber, C. M. *Nano Lett.* **2010,** *10,* 1098.

(6) Schedin, F.; Geim, A. K.; Morozov, S. V.; Hill, E. W.; Blake, P.; Katsnelson, M. I.; Novoselov, K. S. *Nat. Mater.* **2007,** *6,* 652.

(7) Ruoff, R. *Nat. Nanotechnol.* **2008,** *3,* 10.

(8) Dreyer, D. R.; Park, S.; Bielawski, C. W.; Ruoff, R. S. *Chem. Soc. Rev.* **2010,** *39,* 228.

(9) Sessi, P.; Guest, J. R.; Bode, M.; Guisinger, N. P. *Nano Lett.* **2009,** *9,* 4343.

(10) Balog, R.; Jorgensen, B.; Nilsson, L.; Andersen, M.; Rienks, E.; Bianchi, M.; Fanetti, M.; Laegsgaard, E.; Baraldi, A.; Lizzit, S.; Sljivancanin, Z.; Besenbacher, F.; Hammer, B.; Pedersen, T. G.; Hofmann, P.; Hornekaer, L. *Nat. Mater.* **2010,** *9,* 315.

(11) Elias, D. C.; Nair, R. R.; Mohiuddin, T. M. G.; Morozov, S. V.; Blake, P.; Halsall, M. P.; Ferrari, A. C.; Boukhvalov, D. W.; Katsnelson, M. I.; Geim, A. K.; Novoselov, K. S. *Science* **2009,** *323,* 610.

(12) Bekyarova, E.; Itkis, M. E.; Ramesh, P.; Berger, C.; Sprinkle, M.; de Heer, W. A.; Haddon, R. C. *J. Am. Chem. Soc.* **2009,** *131,* 1336.

(13) Chen, W.; Chen, S.; Qi, D. C.; Gao, X. Y.; Wee, A. T. S. *J. Am. Chem. Soc.* **2007,** *129,* 10418.

(14) Wang, X. R.; Li, X. L.; Zhang, L.; Yoon, Y.; Weber, P. K.; Wang, H. L.; Guo, J.; Dai, H. J. *Science* **2009,** *324,* 768.

(15) Green, A. A.; Hersam, M. C. *Nano Lett.* **2009,** *9,* 4031.

(16) Li, X. L.; Wang, X. R.; Zhang, L.; Lee, S. W.; Dai, H. J. *Science* **2008,** *319,* 1229.

(17) Wang, X. R.; Tabakman, S. M.; Dai, H. J. *J. Am. Chem. Soc.* **2008,** *130,* 8152.

(18) Masubuchi, S.; Ono, M.; Yoshida, K.; Hirakawa, K.; Machida, T. *Appl. Phys. Lett.* **2009,** *94,* No. 082107.

(19) Weng, L. S.; Zhang, L. Y.; Chen, Y. P.; Rokhinson, L. P. *Appl. Phys. Lett.* **2008,** *93,* No. 093107.

(20) Tapaszto, L.; Dobrik, G.; Lambin, P.; Biro, L. P. *Nat. Nanotechnol.* **2008,** *3,* 397.

(21) Wei, Z.; Wang, D.; Kim, S.; Kim, S.-Y.; Hu, Y.; Yakes, M. K.; Laracuente, A. R.; Dai, Z.; Marder, S. R.; Berger, C.; King, W. P.; de Heer, W. A.; Sheehan, P. E.; Riedo, E. *Science* **2010,** *328,* 1373.

(22) Wang, Q. H.; Hersam, M. C. *Nat. Chem.* **2009,** *1,* 206.

(23) Lauffer, P.; Emtsev, K. V.; Graupner, R.; Seyller, T.; Ley, L. *Phys. Status Solidi B* **2008,** *245,* 2064.

(24) Huang, H.; Chen, S.; Gao, X. Y.; Chen, W.; Wee, A. T. S. *ACS Nano* **2009,** *3,* 3431.

(25) Foley, E. T.; Yoder, N. L.; Guisinger, N. P.; Hersam, M. C. *Rev. Sci. Instrum.* **2004,** *75,* 5280.

(26) Kaneda, Y.; Stawasz, M. E.; Sampson, D. L.; Parkinson, B. A. *Langmuir* **2001,** *17,* 6185.

(27) Hersam, M. C.; Guisinger, N. P.; Lyding, J. W. *Nanotechnology* **2000,** *11,* 70.

(28) Walsh, M. A.; Hersam, M. C. *Annu. Rev. Phys. Chem.* **2009,** *60,* 193.

(29) Yoder, N. L.; Fakonas, J. S.; Hersam, M. C. *J. Am. Chem. Soc.* **2009,** *131,* 10059.

(30) Basu, R.; Guisinger, N. P.; Greene, M. E.; Hersam, M. C. *Appl. Phys. Lett.* **2004,** *85,* 2619.

(31) Ritter, K. A.; Lyding, J. W. *Nat. Mater.* **2009,** *8,* 235.